Available online at www.sciencedirect.com
ScienceDirect
Journal of Computational Physics 227 (2008) 1701–1721
JOURNAL OF COMPUTATIONAL PHYSICS
www.elsevier.com/locate/jcp

Enriched multi-point flux approximation for general grids

Qian-Yong Chen [a,*,1], Jing Wan [b], Yahan Yang [b], Rick T. Mifflin [b]

[a] *Institute for Mathematics and its Applications, University of Minnesota, 207 Church Street S.E., Minneapolis, 55455-0134, United States*
[b] *ExxonMobil Upstream Research Company, Houston, TX, United States*

Received 26 October 2006; received in revised form 13 September 2007; accepted 25 September 2007
Available online 6 October 2007

Abstract

It is well known that the two-point flux approximation, a numerical scheme used in most commercial reservoir simulators, has $O(1)$ error when grids are not **K**-orthogonal. In the last decade, the multi-point flux approximations have been developed as a remedy. However, non-physical oscillations can appear when the anisotropy is really strong. We found out the oscillations are closely related to the poor approximation of pressure gradient in the flux computation.

In this paper, we propose the control volume enriched multi-point flux approximation (EMPFA) for general diffusion problems on polygonal and polyhedral meshes. Non-physical oscillations are not observed for realistic and strongly anisotropic heterogeneous material properties described by a full tensor. Exact linear solutions are recovered for grids with non-planar interfaces, and a first and second order convergence are achieved for the flux and scalar unknowns, respectively.

Keywords: Anisotropy; Control volume; Heterogeneous; Full tensor diffusion; MPFA

1. Introduction

Many physical processes, for example, the Darcy flow in porous media and the heat transfer in Basin modeling, can be modeled by a diffusion equation in the form

$$-\nabla \cdot \mathbf{K}\nabla p = f. \tag{1}$$

The diffusion coefficient **K** is often a space dependent full tensor because of the strongly anisotropic and inhomogeneous media, which imposes a great challenge for numerical schemes, especially when the principal directions of **K** are not aligned with the grids. This is usually the case for unstructured meshes. In the following, we will state everything in the context of reservoir simulation, simply because the initial motive is to develop a more robust discretization for simulating multi-phase flows in porous media, although the proposed scheme

* Corresponding author. Present address: Department of Mathematics and Statistics, University of Massachusetts Amherst, 710 North Pleasant Street, Amherst 01003-9305, United States. Tel.: +1 413 545 9611; fax: +1 413 545 1801.
E-mail address: qchen@math.umass.edu (Q.-Y. Chen).
[1] Partially funded by ExxonMobil Upstream Research Company.

0021-9991/$ - see front matter © 2007 Elsevier Inc. All rights reserved.
doi:10.1016/j.jcp.2007.09.021

can apply to general diffusion problems described by Eq. (1). In this paper, we assume **K** is a piecewise constant tensor. The scalar unknown p will be called pressure for convenience.

There has been extensive research on developing numerical schemes for Eq. (1) on general grids. Some highly desirable properties of the discretization beyond the classical stability and accuracy, include local mass conservation, harmonic average transmissibilities, discrete maximum principle, and cost-efficiency. For historic reasons, the two-point flux approximation (TPFA), a scheme that is inconsistent when the grids are not **K**-orthogonal, is still used in most commercial reservoir simulators. Roughly speaking, **K**-orthogonality means that the flux $-\mathbf{K}\nabla p \cdot \mathbf{n}$ can be approximated by a factor of the pressure difference from two neighbouring control volumes (see (8) for one example). Unfortunately, **K**-orthogonality is often lost in the grids that honor the geologic features such as the sloping faults and channels, and other important features such as nearly horizontal wells [18]. Recently, Wu and Parashkevov studied the effect of non-orthogonality error of deviated grids on the flow solutions from the two-point flux, control volume method [35]. They concluded that for most practical cases the errors in horizontal flow are relatively small and the errors in vertical flow can be rather significant.

To obtain a consistent scheme, different groups of researchers have independently developed the so-called control volume multi-point flux approximation (MPFA), such as Aavatsmark et al [3], Edwards and Rogers [15], Verma and Aziz [34]. Since their pioneer work, a whole class multi-point flux methods have been developed [2,19,26]. In Ref. [22], the authors implement the multi-point flux methods on a hexahedral grid. More recently, Klausen and Russell [19] compare the multi-point flux approximation with several other locally conservative schemes which handle discontinuous coefficients, such as the classical mixed finite element method and the support operators method (also called mimetic finite difference method). Klausen and Winther also proved the convergence of the multi-point flux approximations on smooth quadrilateral grids [20].

In most cases, good results are obtained by the multi-point flux methods, but non-physical oscillations can appear for strongly anisotropic fields because of non-monotonicity of the matrix (see, e.g. [24,27]). This means that the numerical solution does not satisfy the maximum principle, although the analytical solution does. In order to improve the monotonicity property, Nordbotten and Eigestad recently developed a MPFA Z-method for quadrilateral grids by choosing a different stencil when computing the flux [29]. But it is not clear how to extend their method to unstructured polyhedral meshes. Some other very recent research on this issue includes [23,28,17,4].

The mimetic finite difference schemes proposed by Shashkov et al. [33] are very promising in terms of dealing with highly distorted grids and heterogeneous media. The convergence and super convergence [6,7] are also established for smooth problems on smooth meshes by rewriting the scheme into the form of mixed finite element methods. (A more general proof was provided in Ref. [8].) Furthermore, in Ref. [9], Brezzi et al. employ an innovative technique to generalize it to a family of schemes with parameters which might be tuned to achieve the discrete maximum principle. But by now such a scheme still does not exist, and the computational cost of the mimetic finite difference schemes is an issue too.

There is also considerable advance in mixed finite element type methods for distorted general meshes [10,12], but they are quite expensive and the 3-D case is still under development [25,21]. A worthy alternative, the control volume finite element (CVFE) methods (often called finite volume element methods) [5,11,32], are locally mass conservative and applicable on flexible grids, but they do not handle discontinuous diffusion coefficients well [14].

In this paper, we develop a new multi-point flux approximation method, called enriched multi-point flux approximation (EMPFA), based on more consistent pressure approximations in the interaction region. The proposed method does not produce oscillatory solutions and works for general matching or non-matching polygonal and polyhedral meshes, including meshes with non-planar interfaces. Expected convergence rate is also achieved for the new method, Moreover, the enriched multi-point flux approximation is equivalent to the two-point flux approximation for the **K**-orthogonal grids.

The remaining of the paper is organized as follows. In Section 2, we restate the original multi-point flux approximation on quadrilateral grids. Section 3 describes our new multi-point flux approximation for two-dimensional grids, shows its numerical convergence, and compares the numerical results with the multi-point flux approximation method. In Section 4, we extend the technique in Section 3 to polyhedral meshes. Finally, we summarize the paper and make some concluding remarks in Section 5.

2. Multi-point flux approximation

In this section, we first briefly review the multi-point flux method with surface mid-points as continuity points (called O-method [2]) on quadrilateral grids. The extension to unstructured grids is trivial. Then we analyze the limitations of the MPFA-O method.

2.1. Description of multi-point flux approximation

Let $\Omega \in R^2$ be the computational domain, and divide it into non-overlapping quadrilateral control volumes $\Omega = \cup V_i$. Consider Eq. (1) with piecewise constant permeability $\mathbf{K}$ (i.e. constant on each V_i). In the control volume multi-point flux approximation methods, the mass is conserved on each control volume, i.e. integrate the equation on control volumes $\{V_i\}$ to obtain

$$-\int_{\partial V_i} \mathbf{K}\nabla p \cdot \mathbf{n}\,\mathrm{d}S = \int_{V_i} f\,\mathrm{d}V, \quad \forall V_i, \tag{2}$$

where the left hand side is the amount of flux (i.e. $-\mathbf{K}\nabla\, p \cdot \mathbf{n}$) across the boundary of V_i.

In the MPFA method, there is only one degree-of-freedom (usually pressure at the mass center) for each control volume. The fluxes across control volume interfaces are computed for each interaction region and expressed in terms of those degrees-of-freedom. When computing the fluxes, each interface (a line segment) is divided into two parts, on which the fluxes are first computed separately and then summed up to be the flux across the whole interface. For example, Fig. 1 shows four control volumes with centers C_i's which meet at point O. The polygon area formed by the cell centers C_i's and the edge middle points M_i's is called *interaction region*. The small quadrilateral of each control volume included in the interaction region is called *sub-volume*, e.g. $M_1OM_4C_1$. (Note that each vertex of the mesh corresponds to an interaction region.) In this interaction region, only the fluxes across half edges OM_i's will be computed. Then we loop over all the interaction regions to compute the fluxes for all the control volume boundaries/interfaces.

In order to compute the fluxes across OM_i's (i.e. the integral of $-\mathbf{K}\nabla p \cdot \mathbf{n}$ on OM_i), the values of p at M_i's are introduced as four temporary unknowns. The method with this choice is called the MPFA-O method. (One could also use the values of p at other points as the temporary unknowns.) Recall that the primary unknowns are the values of p at C_i's. With both primary and temporary unknowns, we can compute ∇p and then the fluxes by assuming p is a linear function on the shaded triangles in Fig. 1. For example, when computing the flux across OM_1 and OM_4 from volume C_1, a constant gradient $\nabla\, p$ is computed from the linear function on $\Delta_{M_1M_4C_1}$, and then extrapolated to be the gradient on the whole quadrilateral sub-volume $M_1OM_4C_1$. Hence the flux across OM_1 and OM_4 can be written into the form of $\mathbf{a}^{\mathrm{T}}\mathbf{K}_1\nabla p$ with the area vector $\mathbf{a} = |OM_1|\mathbf{n}_1$ and $-|OM_4|\mathbf{n}_4$ respectively, where $\mathbf{K}_1$ is the diffusion tensor on volume C_1.

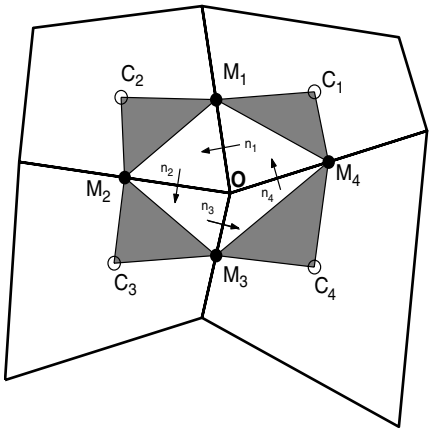

Fig. 1. Multi-point flux method: interaction region.

Denote $\mathbf{P} = (p_{C_1}, p_{C_2}, p_{C_3}, p_{C_4})^{\mathrm{T}}$ and $\overline{\mathbf{P}} = (p_{M_1}, p_{M_2}, p_{M_3}, p_{M_4})^{\mathrm{T}}$, where p_A represents the value of p at point A. Rewrite the fluxes across half edges OM_i's from volume C_i's into a matrix vector product form as $\mathbf{A}\overline{\mathbf{P}} + \mathbf{B}\mathbf{P}$, and the fluxes from the opposite volumes as $\mathbf{C}\overline{\mathbf{P}} + \mathbf{D}\mathbf{P}$. The formula for matrices **A, B, C, D** can be found in [2]. Balancing the fluxes across OM_i's from both sides yields

$$\mathbf{A}\overline{\mathbf{P}} + \mathbf{B}\mathbf{P} = \mathbf{C}\overline{\mathbf{P}} + \mathbf{D}\mathbf{P}.$$

From the above equation, $\overline{\mathbf{P}}$ can be solved in terms of $\mathbf{P}$, and then substituted back to the flux expression. In the end, the fluxes across the half edges can be written as

$$\mathbf{T}\mathbf{P} = [\mathbf{A}(\mathbf{A} - \mathbf{C})^{-1}(\mathbf{D} - \mathbf{B}) + \mathbf{B}]\mathbf{P},$$

where the matrix $\mathbf{T}$ is called the transmissibility matrix in petroleum industry.

Note that the MPFA-O method also applies to both matching and non-matching unstructured polygon grids as shown in Fig. 2, although the above description is only for quadrilateral meshes.

2.2. Limitations of MPFA-O method

In most cases, good results are obtained from the multi-point flux methods. However, non-physical oscillations can appear when the anisotropy of permeability field is strong (see Section 3.4 or Refs. [24,27]). Most researchers agree that the oscillations are due to the non-monotonicity of the matrix. In the following, we do a non-rigorous analysis from the aspect of accuracy, which leads to the development of our new multi-point flux method in the next section.

Consider an interaction region of rectangular control volumes as shown in Fig. 3. As described in the previous section, a linear pressure is assumed on $\Delta_{M_1M_4C_1}$ in the multi-point flux approximation method. It yields a constant pressure gradient as

$$\begin{cases} u = \frac{p_{C_1} - p_{M_1}}{\Delta x}, \\ v = \frac{p_{C_1} - p_{M_4}}{\Delta y}, \end{cases}$$

in which Δx and Δy are the grid size in the x- and y-direction. This pressure gradient is then extrapolated to the whole quadrilateral $M_1OM_4C_1$ and used to compute the fluxes across edges OM_1 and OM_4 from control volume C_1. From the Taylor expansion at point M_1, one can have

$$\left.\frac{\partial p}{\partial y}\right|_{M_1} = v + \Delta x \left.\frac{\partial^2 p}{\partial x \partial y}\right|_{M_1} + O(\Delta y + (\Delta x)^2). \tag{3}$$

Clearly, v will be a poor approximation of $\frac{\partial p}{\partial y}$ at point M_1 if $\frac{\partial^2 p}{\partial x \partial y} \sim \frac{1}{\Delta x}$ in the neighbourhood of M_1. Similar result holds for u being an approximation of $\frac{\partial p}{\partial x}$ at point M_4. We believe that these poor approximations of fluxes due to the built-in extrapolation in the MPFA method contribute to the non-physical oscillations. If the grid is fine enough in the sense of $\Delta x \frac{\partial^2 p}{\partial x \partial y}$ being small near point M_1, the oscillation should be less severe. It is confirmed by the first example in Section 3.4.

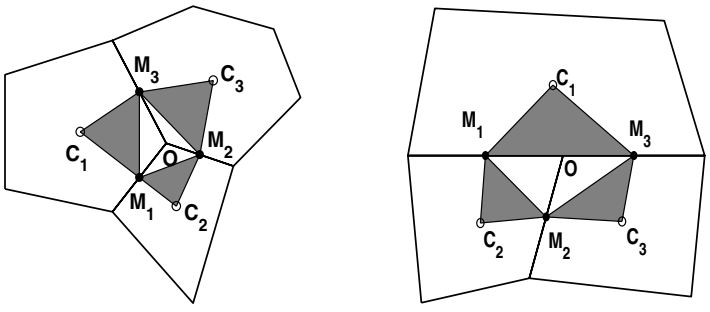

Fig. 2. General two-dimensional grids.

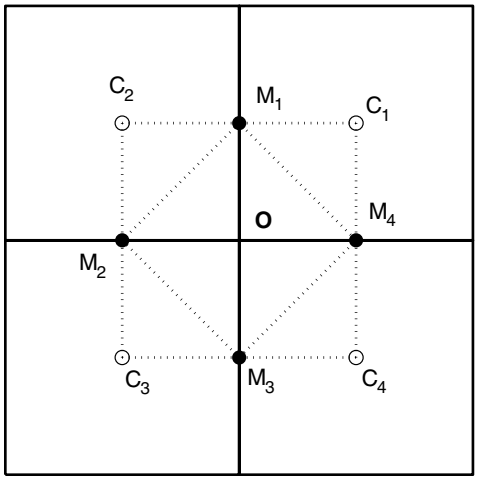

Fig. 3. An interaction region of rectangular control volumes.

Note that these poor approximations do NOT come into the formulation of fluxes when the grid is **K**-orthogonal. It explains why no oscillation was observed for **K**-orthogonal grids.

3. Enriched multi-point flux approximation on polygon meshes

In this section, we present a new multi-point flux approximation, called enriched multi-point flux approximation. It works for general polygon meshes like the multi-point flux approximation. All the descriptions and explanations are only for quadrilateral control volumes, with straightforward extension to unstructured grids. All the notations will be the same as those in Section 2 if not specified otherwise.

3.1. Description

The enriched multi-point flux approximation method follows the same framework as the MPFA-O method: introducing some temporary unknowns in the beginning in order to compute the gradient of p, and then eliminating them by balancing fluxes. But in the EMPFA method we include one more temporary unknown, p at the 'center' of interaction region, to avoid the extrapolation procedure in the MPFA method which has been previously shown to contribute to the non-physical oscillations.

We propose two different approximations for the scalar unknown p. As shown in the left of Fig. 4, the first approximation is a piecewise linear function which is linear on each triangle (e.g. M_1OC_1). Note that only the interaction region is drawn. The second option is to approximate p with a piecewise bilinear function on each quadrilateral in the right of Fig. 4. The bilinear interpolation is included in Appendix A for completeness. With either approximation for p, we compute the fluxes across edges OM_i's and balance them to get a system of four equations written as

$$\mathbf{A}\overline{\mathbf{P}} + \mathbf{B}\mathbf{P} + p_O \cdot \vec{\mathbf{l}} = \mathbf{C}\overline{\mathbf{P}} + \mathbf{D}\mathbf{P} + p_O \cdot \vec{\mathbf{r}}. \tag{4}$$

Note that matrices **A**, **B**, **C**, **D** may have different entries from those in Section 2. For simplicity, the explicit formula for vectors $\vec{\mathbf{l}}$ and $\vec{\mathbf{r}}$ are not given. The new temporary unknown p_O, the value of p at point O, comes into the formulation of fluxes as a result of approximating p in a richer space (compared to the multi-point flux approximation). When the bilinear approximation is chosen, the gradient of p is not a constant on the half edges OM_i's except for some special grids. In this case, a single point quadrature (e.g. M_i) can be used to compute the integral of fluxes on the half edges.

In order to eliminate all the five temporary unknowns, one more equation besides Eq. (4) is needed. We propose two different ways to obtain the extra equation.

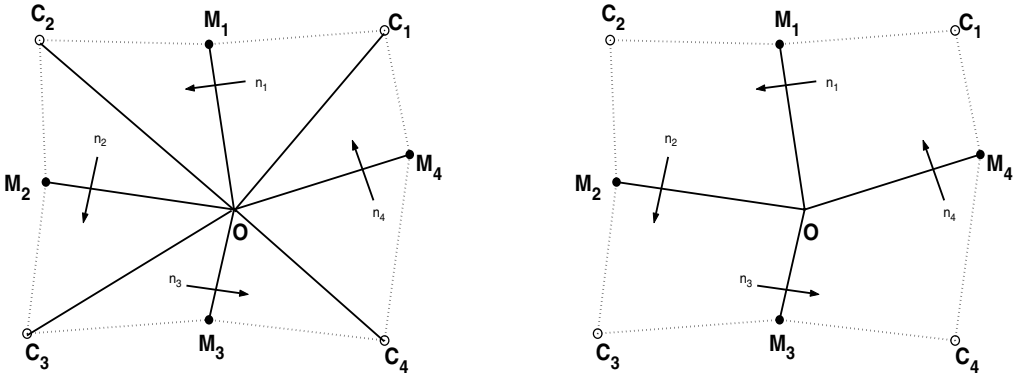

Fig. 4. EMPFA interaction region. Left: piecewise linear approximation. Right: piecewise bilinear approximation.

The first approach is to solve Eq. (1) on a small volume surrounding the interaction region center. We only describe this approach with bilinear approximations of pressure p. The procedure is similar for the piecewise linear approximation. In Fig. 5, $\Omega_\epsilon = D_1D_2D_3D_4$ with $|OD_i| = \epsilon|OM_i|$ is the small volume on which Eq. (1) will be solved, where ϵ is a small positive number. So

$$-\int_{\partial\Omega_\epsilon} \mathbf{K}\nabla p \cdot \mathbf{n}\,\mathrm{d}S = \int_{\Omega_\epsilon} f\,\mathrm{d}V, \tag{5}$$

where $\partial\Omega_\epsilon = D_1D_2 \cup D_2D_3 \cup D_3D_4 \cup D_4D_1$. Note that we only show the small volume for the case with piecewise bilinear pressures.

Consider the edge D_4D_1. After obtaining the bilinear transformation coefficients for the quadrilateral $M_1OM_4C_1$ as described in Appendix A, the flux across edge D_4D_1 can be computed as

$$-\epsilon \cdot \frac{1}{a_2b_3 - a_3b_2}\begin{pmatrix} b_3 - b_2 & a_2 - a_3 \end{pmatrix}\mathbf{K}_1\begin{pmatrix} b_3 & -b_2 \\ -a_3 & a_2 \end{pmatrix}\begin{pmatrix} -1 & 1 & 0 & 0 \\ -1 & 0 & 0 & 1 \end{pmatrix}\begin{pmatrix} p_{M_1} \\ p_O \\ p_{M_4} \\ p_{C_1} \end{pmatrix} + \mathrm{O}(\epsilon^2). \tag{6}$$

In the same way, we compute the flux across other edges of $\partial\Omega_\epsilon$. Therefore, the left hand side of Eq. (5) is equal to

$$\epsilon g(p_O, \mathbf{P}, \overline{\mathbf{P}}) + \mathrm{O}(\epsilon^2), \tag{7}$$

with the explicit expression of g being computed from the sum of Eq. (6) for all Ω_ϵ edges.

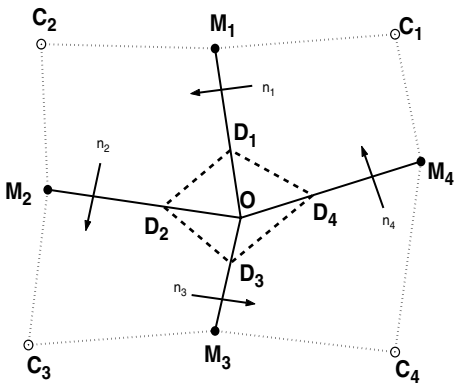

Fig. 5. EMPFA interaction region: a small volume.

Now we consider the right hand side of Eq. (5). Assume f is a square integrable function on a volume $\tilde{\Omega} \supset \Omega_\epsilon$ for some $\epsilon > 0$, i.e.

$$\left(\int_{\tilde{\Omega}} |f|^2 \mathrm{d}V\right)^{1/2} < \infty.$$

By the dominated convergence theorem [31], we have

$$\left(\int_{\Omega_\epsilon} |f|^2 \mathrm{d}V\right)^{1/2} \to 0 \quad \text{as } \epsilon \to 0.$$

Rewrite it into the standard asymptotic notation

$$\left(\int_{\Omega_\epsilon} |f|^2 \mathrm{d}V\right)^{1/2} = \mathrm{o}(\epsilon^0).$$

According to the Schwarz inequality, we have

$$\left|\int_{\Omega_\epsilon} f \,\mathrm{d}V\right| \leqslant \left(\int_{\Omega_\epsilon} |f|^2 \mathrm{d}V\right)^{1/2} \cdot \left(\int_{\Omega_\epsilon} 1 \,\mathrm{d}V\right)^{1/2} = \mathrm{o}(\epsilon).$$

Combining the above equation with Eq. (7), one can have

$$\epsilon g(p_O, \mathbf{P}, \overline{\mathbf{P}}) + \mathrm{O}(\epsilon^2) = \mathrm{o}(\epsilon).$$

Let $\epsilon \to 0$ to obtain the final equation

$$g(p_O, \mathbf{P}, \overline{\mathbf{P}}) = 0,$$

from which we can solve p_O in terms of $\mathbf{P}$ and $\overline{\mathbf{P}}$. Then we can compute the fluxes by solving $\overline{\mathbf{P}}$ in terms of $\mathbf{P}$ in the same way as in the multi-point flux approximation.

Remark 1. The resultant equation is in some sense independent of the shape of Ω_ϵ because of the limiting process. One may be able to eliminate p_O without letting $\epsilon \to 0$. But the formulation will not be as neat as the one we get here.

Remark 2. Although we state our algorithm for an interaction region with four sub-volumes, it works for any interaction region from general two-dimensional grids.

The second approach is to solve the original equation (i.e. Eq. (1)) on the whole interaction region with the standard Finite Element Method (FEM). The mesh can be either one shown in Fig. 4, depending on which approximation is used for p. Dirichlet boundary conditions are imposed, and a linear p is interpolated from its values at two ending points for each boundary line segment connecting C_i's and M_i's. From this FEM solve, the extra unknown p_O can be expressed as a linear function of $\overline{\mathbf{P}}$ and $\mathbf{P}$, which is then inserted into Eq. (4) to eliminate all the other temporary unknowns. After the elimination, the fluxes will be functions of the primary unknowns only, like those in the multi-point flux approximation methods.

One can combine the linear or bilinear approximation with either approach to obtain the extra equation. Almost equivalent numerical results were obtained for the two different approximations.

Note that the enriched multi-point approximation method works for both matching and non-matching unstructured polygon grids. In the following, we show how to make our algorithm work for non-matching grids.

3.2. Non-matching grids

When a linear pressure is assumed, the enriched multi-point flux approximation automatically works for non-matching grids. Only for the bilinear pressure interpolation we need to make a minor change of the above algorithm. Consider a typical interaction region with a non-matching grid point as shown in Fig. 6. Since

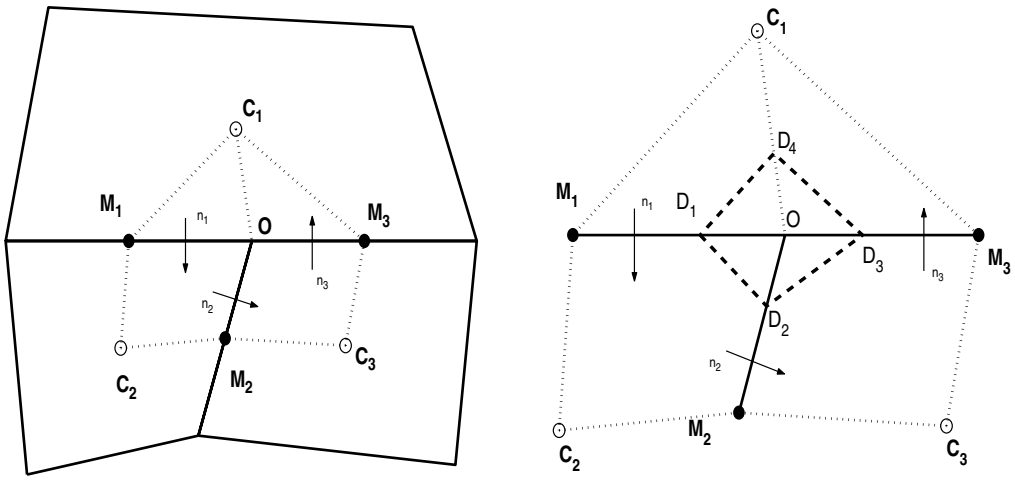

Fig. 6. Interaction region with non-matching grid point. $|OD_i| = \epsilon|OM_i|$, $i = 1, 2, 3$; $|OD_4| = \epsilon|OC_1|$.

$C_1M_1OM_3$ is a degenerated quadrilateral, the point O will be a singularity point if we still use the bilinear transformation to map it to a standard square element. So instead of treating $C_1M_1OM_3$ as one sub-volume, we decompose it into two triangles: ΔC_1M_1O and ΔC_1OM_3, on each of which a linear interpolation is applied. Then following the procedure described in the previous sections, we can compute the flux across all the edges in the interaction region. The small volume used to generate the extra equation to eliminate p_O is shown on the right part of Fig. 6.

3.3. Equivalence of EMPFA and TPFA for *K*-orthogonal grids

Here we show that the enriched multi-point flux approximation is equivalent to the conventional two-point flux approximation for **K**-orthogonal grids.

Consider the flux across edge M_1O from volume C_1 in Fig. 5. Note that the point M_1 has coordinate (0, 0) in ξ–η coordinate system (see Appendix A). Using the formula given in Appendix A, the pressure gradient at point M_1 is

$$\frac{1}{a_2b_3 - a_3b_2}\begin{pmatrix} b_3 & -b_2 \\ -a_3 & a_2 \end{pmatrix}\begin{pmatrix} -1 & 1 & 0 & 0 \\ -1 & 0 & 0 & 1 \end{pmatrix}\begin{pmatrix} p_{M_1} \\ p_O \\ p_{M_4} \\ p_{C_1} \end{pmatrix}.$$

Since the grid is **K**-orthogonal, there exists a constant c such that

$$\mathbf{a}^{\mathrm{T}}\mathbf{K} = c\,C_1\vec{M}_1 = c(\,-a_3 \quad -b_3\,). \tag{8}$$

Plug the above two equations into the flux formula $\mathbf{a}^{\mathrm{T}}\mathbf{K}\,\nabla p$ to obtain

$$\mathbf{a}^{\mathrm{T}}\mathbf{K}\nabla p = c(p_{M_1} - p_{C_1}),$$

which is exactly the same formula as that from the two-point flux approximation. Therefore, we have showed that the enriched multi-point flux approximation is equivalent to the conventional two-point flux approximation for **K**-orthogonal grids.

3.4. Numerical experiments

In this section, we solve Eq. (1) for various permeabilities and solutions with different regularities.

3.4.1. Non-physical oscillations

The problem described in Ref. [24] is to solve Eq. (1) with permeability

$$\mathbf{K} = \begin{pmatrix} \cos\theta & \sin\theta \\ -\sin\theta & \cos\theta \end{pmatrix} \begin{pmatrix} k_1 & 0 \\ 0 & k_2 \end{pmatrix} \begin{pmatrix} \cos\theta & -\sin\theta \\ \sin\theta & \cos\theta \end{pmatrix}. \tag{9}$$

The computation domain is $[-0.5, 0.5] \times [-0.5, 0.5]$ with a well sitting in the middle. Constant pressure is used as boundary conditions. A constant flow rate is specified in the code for the control volume including the well. As shown in Figs. 7 and 8, non-physical oscillations are present when k_2/k_1 is large and the grid is not **K**-orthogonal. Fig. 9 shows the solution from the multi-point flux approximation on finer quadrilateral grids. Clearly the oscillation becomes less severe when refining the grid.

Figs. 10 and 11 display the solution from the enriched multi-point flux approximation. No oscillation is observed. For comparison purposes, we also show the pressure profile from the two-point flux approximation. The anisotropic structure of the pressure profile is clearly distorted by the two-point flux approximation.

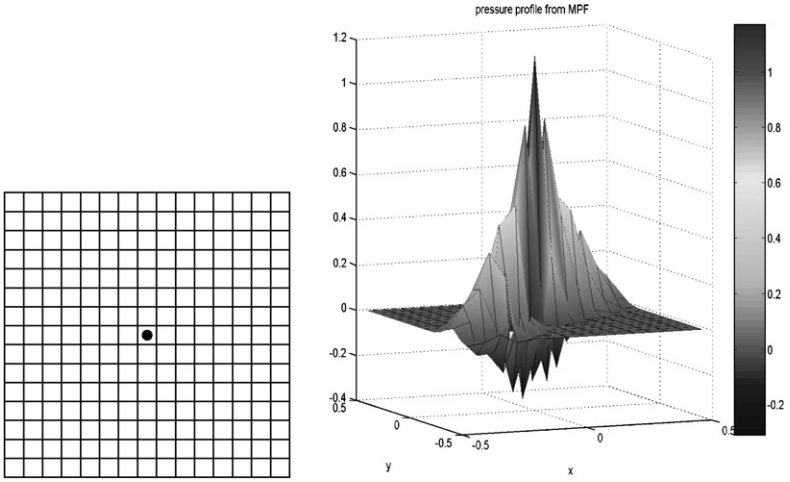

Fig. 7. Oscillatory solution from MPFA on quadrilateral control volumes. $k_1 = 1$, $k_2 = 1000$, $\theta = \pi/3$. Left: grid of size 15×15. Right: pressure profile.

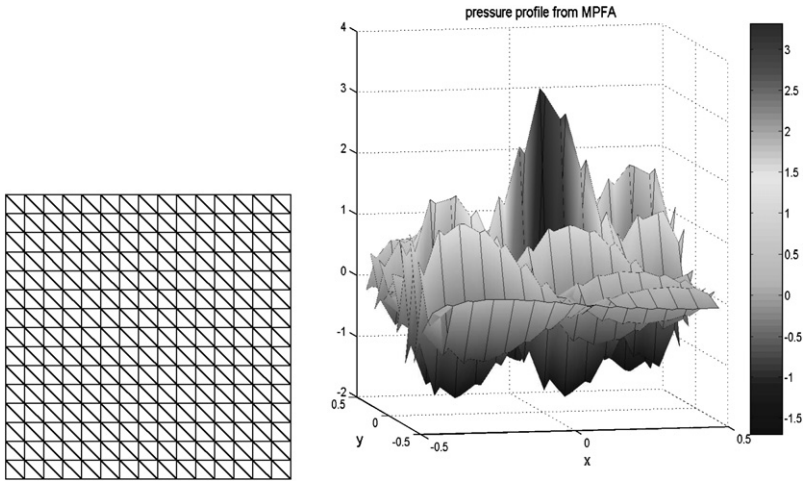

Fig. 8. Oscillatory solution from MPFA on triangular control volumes. $k_1 = 1$, $k_2 = 25$, $\theta = \pi/3$. Left: grid. Right: pressure profile.

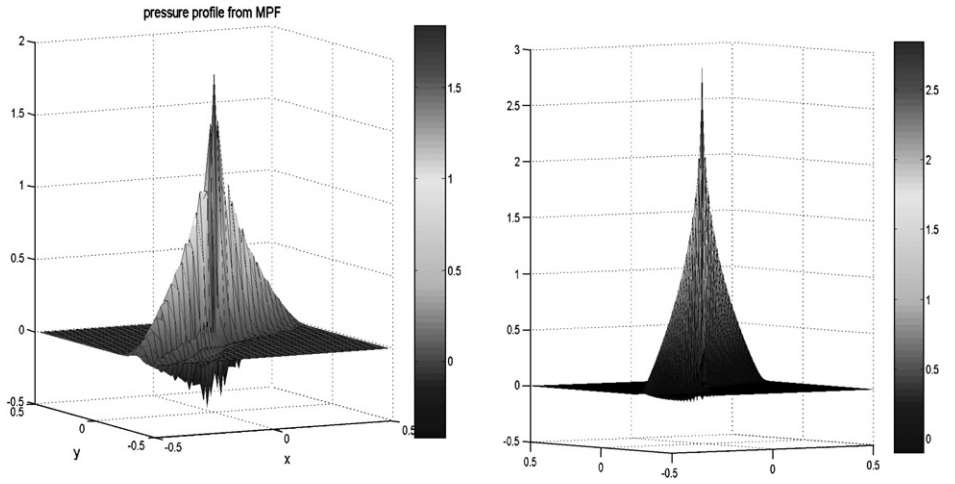

Fig. 9. Less oscillatory solution from MPFA on finer quadrilateral grids. $k_1 = 1$, $k_2 = 1000$, $\theta = \pi/3$. Left: 33×33. Right: 99×99.

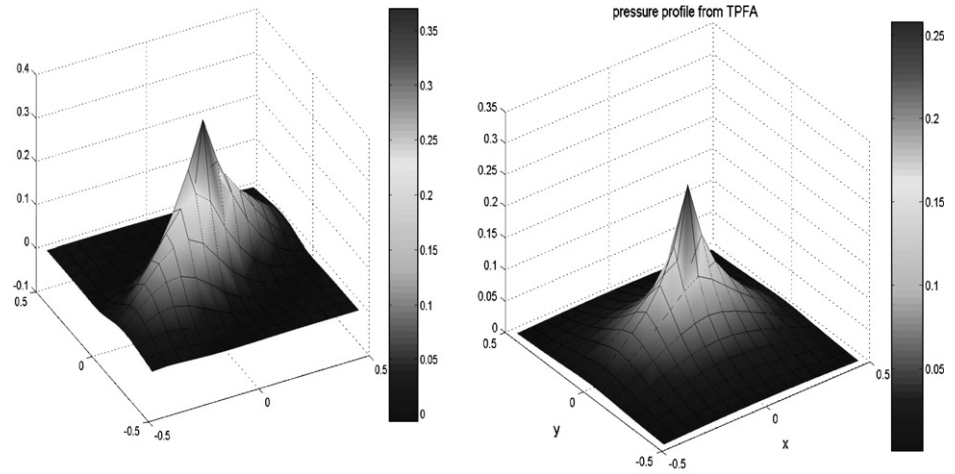

Fig. 10. Pressure profile on the quadrilateral grid. Left: EMPFA. Right: TPFA. $k_1 = 1$, $k_2 = 1000$, $\theta = \pi/3$. Grid: 15×15.

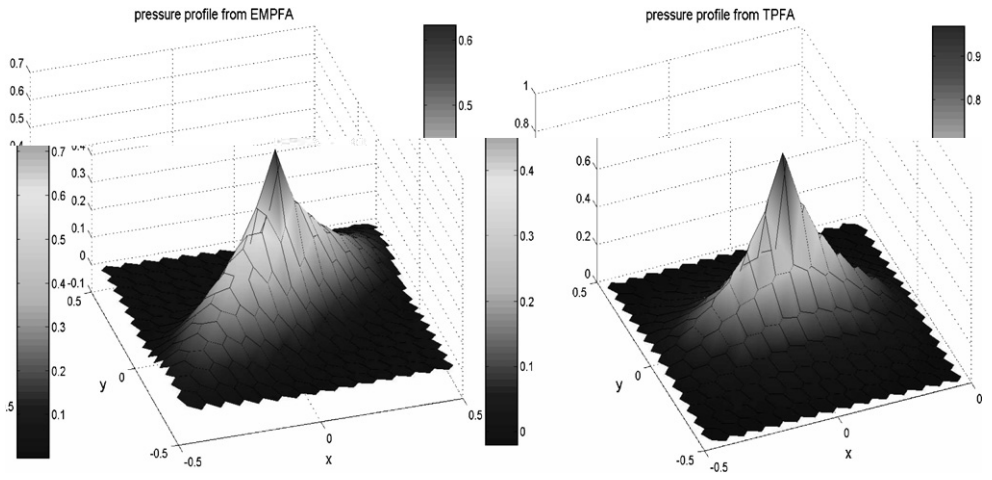

Fig. 11. Pressure profile on the triangular grid. Left: EMPFA. Right: TPFA. $k_1 = 1$, $k_2 = 25$, $\theta = \pi/3$.

In order to have a quantitative comparison between the EMPFA and MPFA methods, we consider a case similar to the above problem. Assume the analytical solution is $p(x, y) = -q\log(r) + c$, where $r = \sqrt{\xi^2 + \eta^2}$ with

$$\begin{pmatrix} \xi \\ \eta \end{pmatrix} = \begin{pmatrix} \frac{1}{\sqrt{k_1}} & \\ & \frac{1}{\sqrt{k_2}} \end{pmatrix} \begin{pmatrix} \cos\theta & -\sin\theta \\ \sin\theta & \cos\theta \end{pmatrix} \begin{pmatrix} x \\ y \end{pmatrix}.$$

The constants q and c are chosen such that $p \geqslant 0$ on the computational domain $[-0.5, 0.5]\times[-0.5, 0.5]$. The permeability tensor is assumed to have the form as given in Eq. (9). Exact solution is applied as Dirichlet boundary conditions. From the result shown in Fig. 12, the enriched multi-point flux method is more accurate than the original multi-point flux method for this test case.

3.4.2. Uniform flow

The analytical solution is a uniform flow on $[-0.5, 0.5]\times[-0.5, 0.5]$. Specially, we choose

$$p(x, y) = x + 4, \quad \text{and} \quad p(x, y) = y + 2.$$

The permeability is assumed to be a diagonal tensor, $\mathbf{K} = \mathrm{diag}(10, 1)$. The computation is done on a pseudo-random grid in Fig. 13. The grid is generated by first building a uniform Cartesian grid and then perturbing it in a certain way such that all the control volumes are still convex quadrilaterals. More details on construction of this type of random grids can be found in [33]. As expected, the exact solution is recovered up to the machine accuracy by the enriched multi-point flux method.

3.4.3. Convergence study

We now study the convergence rate of the enriched multi-point flux approximation. The discrete L_2 error of pressure and normal velocities take the form

$$\begin{cases} ep = \left(\sum_i |V_i|(p_{\mathrm{ex},i} - p_i)^2\right)^{1/2}, \\ ef = \left(\sum_{e\in\mathcal{E}} Q_e \left(\frac{f_{\mathrm{ex},e} - f_e}{|e|}\right)^2 \Big/ \sum_{e\in\mathcal{E}} Q_e\right)^{1/2}, \end{cases}$$

where $\{V_i\}$ is the set of all the control volumes and $\mathcal{E}$ is the set of all the control volume edges. $|V_i|$ denotes the volume (area for 2-D problems) of control volume V_i, while Q_e is the volume associated with edge e. In this

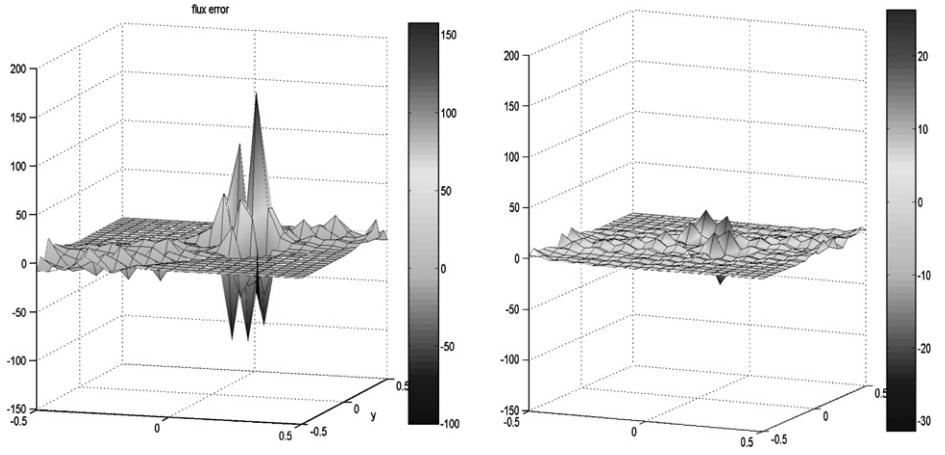

Fig. 12. Flux error. Left: MPFA. Right: EMPFA. $k_1 = 1$, $k_2 = 1000$, $\theta = \pi/3$. Quadrilateral grid of size 11×11.

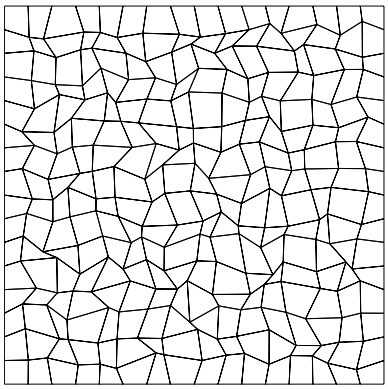

Fig. 13. Random grid.

paper, Q_e is simply the total area of the sub-volumes that share the edge e. The same discrete error measure has been used in Refs. [19,16].

Example 1. The analytical solution $p(x,y) = \cos(\pi x)\cos(\pi y) + 2$ and $\mathbf{K} = \mathrm{diag}(10,1)$. The computation is done on the random grid as shown in Fig. 13. During the grid refinement, we first refine the Cartesian mesh uniformly and then perturb the mesh to obtain a finer random grid. As shown in Table 1, the expected convergence rate is achieved for the enriched multi-point flux method.

Example 2. Consider a case with discontinuous permeability field. Fig. 14 shows the domain including four sub-domains each of which is assumed to have homogeneous isotropic permeability field, i.e. $\mathbf{K}_i = k_i\mathbf{I}$. The four sub-domains meet at the center (origin $(0,0)$) with angle ϕ. We seek an analytical solution with form

$$p(x,y) = p(r,\theta) = r^{\alpha}(a_i \sin(\alpha\theta) + b_i \cos(\alpha\theta)), \quad \text{if } (x,y) \in i\text{th sub-domain}, \quad i = 1,\ldots,4,$$

Table 1
Convergence rate

N	EMPFA				MPFA			
	ep	Rate	*ef*	Rate	*ep*	Rate	*ef*	Rate
8	0.01593		1.4039		0.01892		1.7415	
16	0.00344	2.21	0.6198	1.18	0.00369	2.36	0.7691	1.18
32	0.00082	2.06	0.2702	1.20	0.00100	1.88	0.3851	1.00
64	0.00023	1.81	0.1195	1.18	0.00029	1.78	0.1835	1.07

$p(x, y) = \cos(\pi x)\cos(\pi y) + 2$ and $\mathbf{K} = \mathrm{diag}(10, 1)$.

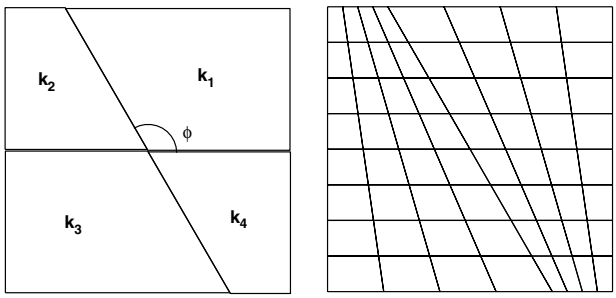

Fig. 14. Discontinuous permeability field. Left: the computation domain. Right: 8×8 mesh which honors discontinuity of permeability.

Table 2
Convergence rate

N	EMPFA				MPFA			
	ep	Rate	*ef*	Rate	*ep*	Rate	*ef*	Rate
8	0.2688		6.5372		0.3360		4.9486	
16	0.1044	1.36	4.1590	0.65	0.1255	1.42	3.1238	0.66
32	0.0393	1.41	2.5827	0.69	0.0454	1.47	1.9380	0.69
64	0.0145	1.44	1.5803	0.71	0.0162	1.49	1.1877	0.71

Permeability $\mathbf{K}_i = k_i\mathbf{I}$ with $k_1 = 100$, $k_2 = 1$, $k_3 = 1$, $k_4 = 1$. $\phi = 2\pi/3$.

in the polar coordinate system. The coefficients a_i's , b_i's and α can be computed from the continuity conditions of pressure p and flux $\mathbf{K}\nabla p \cdot \mathbf{n}$ across the interfaces of sub-domains. When $k_1 = 100$, $k_2 = 1$, $k_3 = 1$, $k_4 = 1$, $\phi = 2\pi/3$, we have a solution with

$$\alpha = 0.7547,$$
$$a_1 = 1.00995, \quad a_i = 1.99990, \qquad i = 2, 3, 4,$$
$$b_1 = 1, \qquad b_i = 100.98019, \quad i = 2, 3, 4.$$

Table 2 lists convergence rates from the enriched multi-point flux method and the multi-point flux method. The order of the L_2 error of pressure is almost $h^{2\alpha}$, which is the optimal rate for conforming finite element methods. (The order $h^{2\alpha}$ is obtained in Ref. [30] with the discontinuous Galerkin method.) We also did the test cases with $\phi = \pi/2$, $k_1 = k_3 = 1$, $k_2 = k_4 = 5$, 10, 100 as Eigestad and Klausen did in Ref. [16]. Similar results were obtained for the enriched multi-point flux approximation.

3.4.4. Discussion

Thorough numerical tests have been done to verify the accuracy of the enriched multi-point flux approximation method. In the above numerical experiments, almost equivalent results have been obtained for both Dirichlet and Neumann boundary conditions, and for any combination of linear/bilinear pressure approximation and either way to get the extra equation (cf Section 3.1). Figs. 15 and 16 list a few other meshes we have tried, some of which are actually exported from the gridding software currently used in ExxonMobil Upstream Research Company. For all the meshes, the exact linear solution can be recovered, and expected convergence is achieved for both the pressures and normal velocities.

We have also done extensive tests on the robustness of the new method. No oscillations were observed in all the numerical solutions when strongly anisotropic $\mathbf{K}$ exists, except for one case a spike appears in the interior domain. In this particular case, the material property (permeability field) is taken from an XZ cross-section of SPE10 [1]. Then we rotate the two-dimensional permeability for 60 degrees in the counterclockwise direction, and use the rotated permeability as $\mathbf{K}$ in the numerical experiment. However, the numerical permeability field is not considered to be realistic or physical because the correlation is completely lost after the artificial rotation. Not surprisingly, the control volume finite element method performs much better in this case because it is essentially a finite element method which usually does not have problem with oscillations.

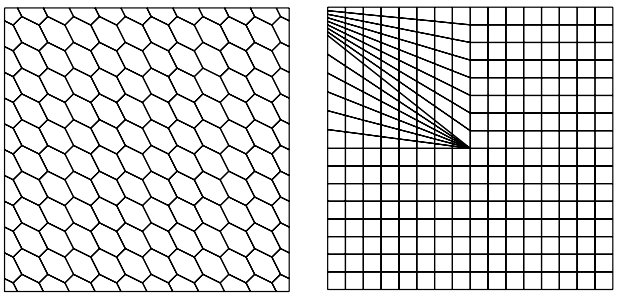

Fig. 15. Two-dimensional meshes I.

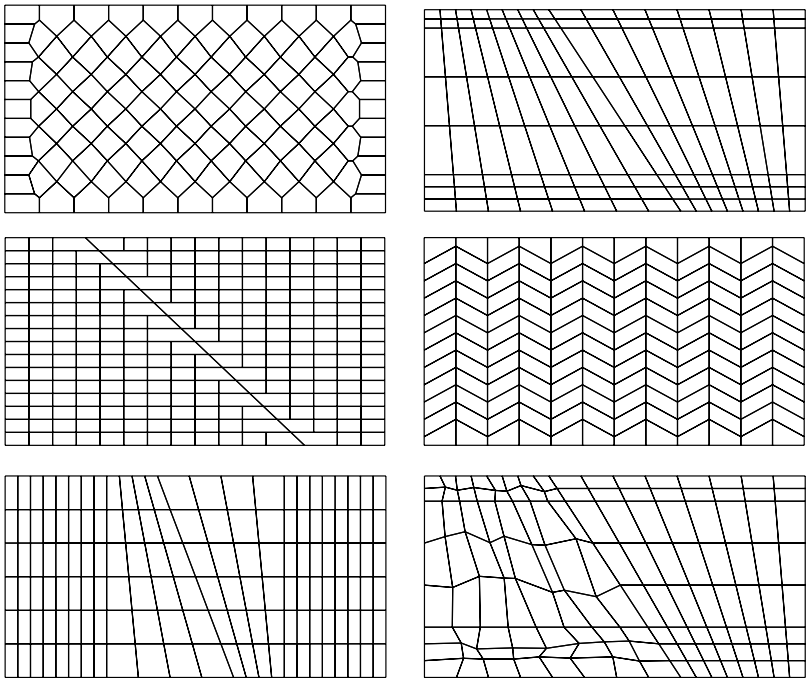

Fig. 16. Two-dimensional meshes II.

4. Enriched multi-point flux approximation for polyhedral meshes

In this section, we extend the enriched multi-point flux approximation method to three-dimensional grids. For simplicity, we only describe the extension with the combination of piecewise linear approximation of pressure and the FEM way of obtaining the extra equation to eliminate the temporary unknown which is located at the 'center' of the interaction region.

4.1. Local mesh

From the description in Section 3.1, the interaction region in 2-D, more precisely every sub-volume, has to be divided into triangles (see Fig. 4) in order to define a piecewise linear approximation for p. Recall that every sub-volume is the portion of one control volume that lies inside the interaction region. For two-dimensional grids, each sub-volume is always a quadrilateral except for the non-matching grids (see e.g. Fig. 6). For unstructured polyhedral grids, the sub-volumes are much more complex, and so are the interaction regions. We first need to divide the interaction regions of three-dimensional meshes into tetrahedrons in order to define a piecewise linear approximation for the scalar unknown p.

Since each sub-volume will be partitioned into tetrahedrons separately, we only explain how to divide one sub-volume. Figs. 17 and 18 demonstrate the whole process of constructing the sub-volume and local mesh for one particular control volume. Suppose point A is the 'center' of the interaction region, i.e. where the control volumes meet. The sub-volume for this control volume is the polyhedron formed by point A, the volume center C, and the centers of the control volume faces and edges which meet at point A. In the graph, the face centers (e.g. B) and edge centers (e.g. D and E) are the dark dots and star-shaped points respectively. Note that the control volume faces could be non-flat. In the implementation, we simply use the average of face vertices as the face center for each face.

Half of the sub-volume faces (e.g. $ADBE$) will be shared with another sub-volume. So when dividing the sub-volume, we have to make sure the partitions of the shared faces are consistent from both sides. This is achieved by a two-step partition strategy. The first step is to divide the sub-volume into pyramids by connect-

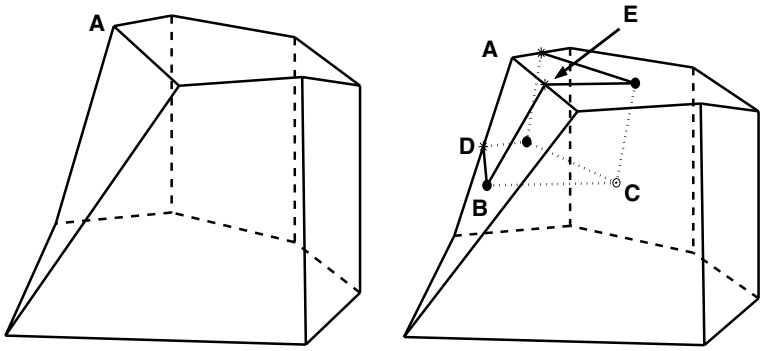

Fig. 17. Polyhedral mesh. Left: a control volume. Right: the corresponding sub-volume.

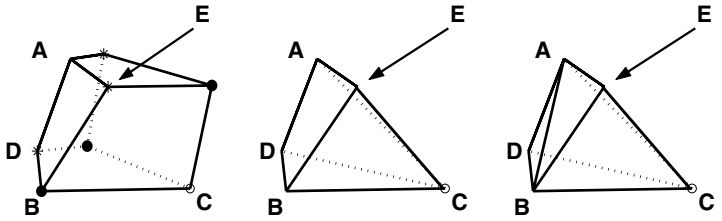

Fig. 18. Polyhedral mesh: construction of local mesh.

ing C with all the edge centers. One such pyramid is shown in the middle part of Fig. 18. The total number of pyramids is equal to the total number control volume faces sharing point A. The second step is to partition each pyramid into two tetrahedrons by connecting point A to one previously computed face center which lies on the bottom of the pyramid (point B in Fig. 18). The resultant two tetrahedrons, $CABE$ and $CABD$, are shown in the right graph of Fig. 18. After the above procedure, each interaction region is divided into several non-overlapping tetrahedrons, on which a piecewise pressure can be defined.

4.2. Computation of flux

Using a piecewise linear approximation for p on the local tetrahedron mesh constructed in the last section, we can compute ∇p and the flux across the interfaces. Clearly the flux formulation will involve the values of p at point A, C, the face and edge centers, among which we only want to keep in our final numerical scheme the primary unknowns, the values of p at the volume centers. Again, like the algorithm for polygon meshes, we can eliminate face center unknowns by balancing fluxes, and remove p_A by using the Finite Element Method to solve the original equation on each individual interaction region. So the only unknowns needing extra work are those located at the control volume edge centers. Bear in mind these unknowns cannot be eliminated through the above local FEM solve because the edge centers are on the boundaries of the corresponding interaction region.

We propose to use both least square and averaging to directly approximate the edge center unknowns by linear functions of volume and face center unknowns. First, we employ a least square method in each sub-volume to obtain a linear p from its values at the volume and face centers. The reason of choosing the least square method is because a three-dimensional linear function has only four coefficients, but in general there may be more than three faces of a control volume meeting at a single point. However, for the sub-volume given in Fig. 18, the least square fitting simply becomes a linear interpolation procedure as there are only three face centers involved (i.e. only three faces of the control volume meet at point A).

With the linear function computed as above for each sub-volume, p at every edge center will have multiple values as each edge center point belongs to more than one sub-volume. We simply use the average of those

values as the final value of p at the edge center. After the averaging, the value of p at any edge center is expressed as a linear function of the values of p at the volume centers and the face centers of all the sub-volumes in the local interaction region.

Combining the above, we propose the enriched multi-point approximation methods as follows.

Algorithm 1 (*EMPFA*).

1. For each vertex of the mesh, construct the interaction region and local mesh as described in Section 4.1.
2. Employ a piecewise linear approximation of p on the mesh built in the first step. Use this approximation to compute the fluxes on each interface from the control volumes on both sides.
3. Solve the original equation with the Finite Element Method on the interaction region for pressure at the 'center' of the interaction region.
4. In each sub-volume, apply the least square method to find a linear function of p from its values at the volume center and face centers.
5. Express the value of p at every edge center in terms of p at all the volume centers and face centers, by averaging the obtained linear functions in all the sub-volumes that contain this edge center point.
6. Use the formula obtained in Steps 2 and 5 to eliminate the pressures at the edge centers and interaction region center from the flux formulation.
7. Eliminate the face center pressures by balancing the fluxes from both sides on each interface. It leads to a flux formulation in terms of the control volume center pressures only.
8. Apply the finite volume method to solve the original equation with the fluxes computed in Step 7. It gives a linear algebraic equation which then can be solved by standard solvers.

4.3. Numerical results

In this section, we solve Eq. (1) with the EMPFA method described in the last section. In particular, we consider two grids given in Fig. 19. These two are actually two-and-a-half dimensional grids in the sense that they are built by first constructing a two-dimensional grid on XY-plane, and then projecting this areal mesh in Z-direction to each layer. Apparently, the areal mesh for the grids in Fig. 19 are quadrilateral and polygon mesh respectively. We also randomly perturb the grids in the vertical direction as

$$z = z + \Delta z \times r \times \mathrm{rand}([-1, 1]), \quad 0 < r < 0.5,$$

where Δz is the grid size and rand($[-1, 1]$) means a uniform random number from $[-1, 1]$. One should note the control volume faces can be non-planar after the random perturbation (see the left graph of Fig. 19).

We choose $2\frac{1}{2}$-D grids because our algorithm is initially developed for reservoir simulations and most current reservoir simulators use only $2\frac{1}{2}$-D grids.

If not specified otherwise, we assume the domain is $[-1, 1]^3$, and the permeability takes the form

$$\mathbf{K} = \mathbf{O}_x^{\mathrm{T}} \Lambda \mathbf{O}_x,$$

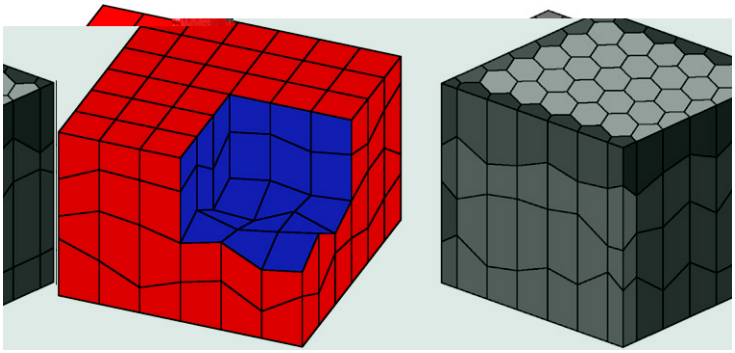

Fig. 19. Two-and-a-half dimensional grids.

where $\Lambda = \mathrm{diag}(10, 10, 1)$ and $\mathbf{O}_x$ is the rotation matrix around x-axis:

$$\mathbf{O}_x = \begin{pmatrix} 1 & 0 & 0 \\ 0 & \cos\theta & \sin\theta \\ 0 & -\sin\theta & \cos\theta \end{pmatrix}.$$

Problem 1 (*Linear flow*). Let the solution be

$$p = x + y + z + 4.$$

The exact solution and flux are recovered for both meshes in Fig. 19 with random perturbation $r = 0.4$.

Problem 2 (*Numerical convergence*). Let the solution be

$$p = \cos(\pi x)\cos(\pi y)\cos(\pi z).$$

The rotation angle is 30 degrees (i.e. $\theta = 30°$) and the perturbation parameter $r = 0.3$.

When refining the mesh, we first refine the mesh uniformly in all the directions, and then perturb the z-coordinates, like all other random meshes. We compute the discrete L^2 error of pressure and normal velocities which take the form

$$\begin{cases} ep &= \left(\sum_i |V_i|(p_{\mathrm{ex},i} - p_i)^2\right)^{1/2}, \\ eu &= \left(\sum_{e\in\mathcal{E}} Q_e \left(\frac{f_{\mathrm{ex},e} - f_e}{|e|}\right)^2 \Big/ \sum_{e\in\mathcal{E}} Q_e\right)^{1/2}, \end{cases}$$

where $\{V_i\}$ is the set of all the control volumes and $\mathcal{E}$ is the set of all the control volume faces. $|V_i|$ denotes the volume of control volume V_i, while Q_e is the volume associated with face e. In this paper, the sum of the area of sub-volumes sharing face e is used as Q_e. The similar discrete error measures is used in Section 3.4.

We also compute the $H(\mathrm{div})_h$ error for the flux, defined as

$$\|\mathbf{u} - \mathbf{u}_h\|_{H(\mathrm{div}),h} = \left(\sum_{\mathrm{all}V_i} \int_{\partial V_i} (\mathbf{u}_h \cdot \mathbf{n} + \mathbf{K}\nabla p \cdot \mathbf{n})^2 \, \mathrm{d}l\right)^{1/2},$$

where u_h denotes the numerical flux. Note that the discrete $H(\mathrm{div})_h$ error is actually computed in the paper by applying certain quadrature rule to the above boundary integral. The results are listed in Table 3 and 4. For completeness, we also give the results from the MPFA-O method in Tables 5 and 6.

Problem 3 (*Horizontal well*). The permeability $\mathbf{K} = \mathbf{O}_x^{\mathrm{T}}\Lambda\mathbf{O}_x$, $\Lambda = \mathrm{diag}(1000, 1000, 1)$ and the rotation angle is 30 degrees. Zero pressure is imposed as boundary conditions.

For this problem, we assume the horizontal well penetrates three control volumes in the center of the computational domain. No well model is involved in the implementation. We simply fix the flow rate for each well block in the code, i.e.

Table 3
Discrete norms of the error

N	ep	Rate	eu	Rate	$\|\mathbf{u} - \mathbf{u}_h\|_{H(\mathrm{div})}$	Rate
2	0.1351		6.2790		11.0248	
4	0.0297	2.18	3.2825	0.94	7.7657	0.51
8	0.0072	2.05	1.4317	1.20	4.5238	0.78
16	0.0018	2.01	0.6645	1.11	2.8617	0.66

Quadrilateral areal mesh. N: number of grid points in each direction.

Table 4
MPFA: discrete norms of the error

N	ep	Rate	eu	Rate	$\|\mathbf{u}-\mathbf{u}_h\|_{H(\mathrm{div})}$	Rate
2	0.1608		7.1225		12.3430	
4	0.0320	2.33	3.6002	0.98	8.2885	0.57
8	0.0078	2.03	1.7936	1.01	5.4665	0.60
16	0.0019	2.02	0.8942	1.00	3.7351	0.55

Quadrilateral areal mesh.

Table 5
Discrete norms of the error

NCell	ep	Rate	eu	Rate	$\|\mathbf{u}-\mathbf{u}_h\|_{H(\mathrm{div})}$	Rate
18	0.0497		6.2519		12.8434	
100	0.0222	1.41	4.2373	0.68	10.6348	0.33
648	0.0068	1.90	2.2228	1.04	7.3477	0.59
4624	0.0019	1.92	1.1290	1.03	5.0205	0.58

Polygonal areal mesh. NCell: total number of control volumes.

Table 6
MPFA: discrete norms of the error

NCell	ep	Rate	eu	Rate	$\|\mathbf{u}-\mathbf{u}_h\|_{H(\mathrm{div})}$	Rate
18	0.0683		6.9493		14.1232	
100	0.0281	1.55	4.8028	0.65	11.7141	0.33
648	0.0080	2.02	2.4910	1.05	8.0036	0.61
4624	0.0022	1.95	1.2863	1.01	5.5824	0.55

Polygonal areal mesh.

$$f(x,y,z)=\begin{cases} c & (x,y,z)\in \text{well block},\\ 0 & \text{otherwise},\end{cases}$$

where c is some constant. The pressure profile is plotted in Fig. 20. Clearly, the solution from the enriched multi-point flux approximation method does not have the non-physical oscillations appearing in the MPFA solution.

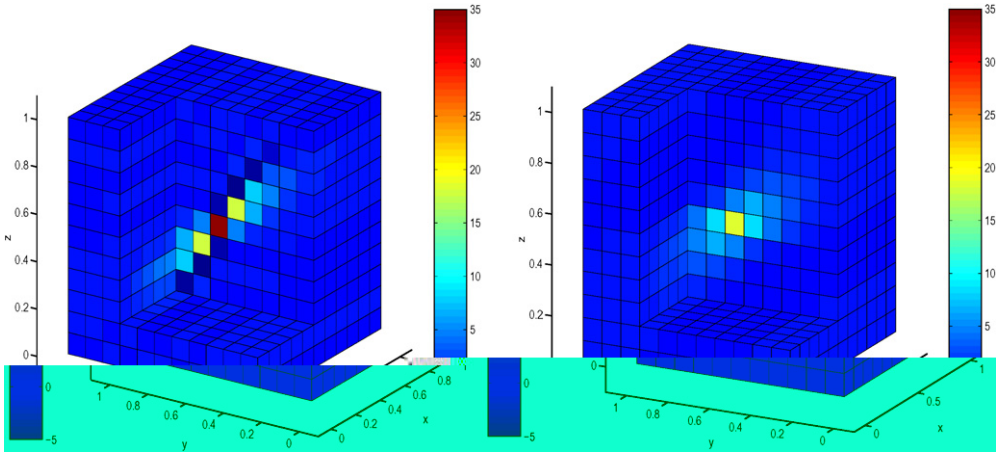

Fig. 20. Pressure from MPFA and EMPFA. Left: MPFA. Right: EMPFA.

5. Summary

The control volume multi-point flux approximation produces oscillatory solutions for diffusion processes in strongly anisotropic media. Within the setting of reservoir simulation, we showed that the oscillations are related to the poor approximation of pressure gradient in flux computation when the second order cross partial derivative of pressure is large. We then developed a new multi-point flux approximation, called enriched multi-point flux approximation (EMPFA), for general polygonal grids including non-matching grids. It is based on a more consistent approximation of pressure, and does not produce oscillatory solutions for strongly anisotropic permeability field, in contrast to other existent schemes such as the multi-point flux approximation method. The expected convergence rate is achieved.

We extended the enriched multi-point approximation method to unstructured polyhedral grids. Besides getting non-oscillating solutions, the EMPFA can also recover the exact linear solution for grids with non-planar interfaces, and compute the scalar and flux unknowns respectively with a first and second convergence on meshes which have perturbations of order $O(h)$.

Acknowledgments

We thank the ExxonMobil Upstream Research Company management for the permission to publish the paper, and appreciate the very fruitful discussions with our colleagues: Bret Beckner, Bill Watts, Adam Usadi, Ilya Mishev, Santosh Verma, Rossen Parashkevov, and Xiao-Hui Wu.

Appendix A. 'Bilinear' interpolation on quadrilaterals

Here, we review the interpolation procedure of the quadrilateral element [13]. This interpolation is not an authentic bilinear interpolation on quadrilaterals. Instead, as shown in Fig. A-1, a quadrilateral $A_1A_2A_3A_4$ is mapped to a standard reference element, $[0, 1]\times[0, 1]$ in ξ–η plane, by a bilinear mapping with the form

$$\begin{cases} x &= x(\xi,\eta) = a_1 + a_2\xi + a_3\eta + a_4\xi\eta, \\ y &= y(\xi,\eta) = b_1 + b_2\xi + b_3\eta + b_4\xi\eta. \end{cases} \tag{A.1}$$

The interpolated function is required to be bilinear on the reference element, i.e.

$$p(x,y) = p(\xi,\eta) = p_1(1-\xi)(1-\eta) + p_2\xi(1-\eta) + p_3\xi\eta + p_4(1-\xi)\eta,$$

where $p_i = p_{A_i}, i = 1,\ldots,4$, denote the values of the original function at point A_i's. The notation is abused a bit by using p to represent the interpolated function.

With simple computation, one can have

$$\begin{cases} a_1 = x_1, \\ a_2 = x_2 - x_1, \\ a_3 = x_4 - x_1, \\ a_4 = x_1 + x_3 - (x_2 + x_4), \end{cases} \qquad \begin{cases} b_1 = y_1, \\ b_2 = y_2 - y_1, \\ b_3 = y_4 - y_1, \\ b_4 = y_1 + y_3 - (y_2 + y_4), \end{cases}$$

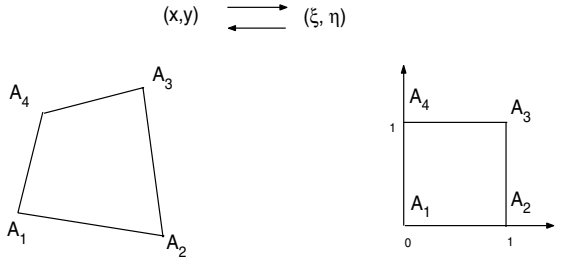

Fig. A-1. From a quadrilateral to a reference element.

where (x_i, y_i) is the coordinates of point A_i in x–y coordinate system. The Jacobian matrix of the mapping takes the form

$$\mathbf{J} = \begin{pmatrix} \frac{\partial x}{\partial \xi} & \frac{\partial y}{\partial \xi} \\ \frac{\partial x}{\partial \eta} & \frac{\partial y}{\partial \eta} \end{pmatrix} = \begin{pmatrix} a_2 + a_4\eta & b_2 + b_4\eta \\ a_3 + a_4\xi & b_3 + b_4\xi \end{pmatrix}.$$

So the gradient of the interpolated function at any point can be computed as

$$\begin{pmatrix} \frac{\partial p}{\partial x} \\ \frac{\partial p}{\partial y} \end{pmatrix} = \frac{1}{\det(\mathbf{J})} \begin{pmatrix} b_3 + b_4\xi & -(b_2 + b_4\eta) \\ -(a_3 + a_4\xi) & a_2 + a_4\eta \end{pmatrix} \cdot \begin{pmatrix} -(1-\eta) & 1-\eta & \eta & -\eta \\ -(1-\xi) & -\xi & \xi & 1-\xi \end{pmatrix} \cdot \begin{pmatrix} p_1 \\ p_2 \\ p_3 \\ p_4 \end{pmatrix}, \tag{A.2}$$

where $\det(\mathbf{J}) = (a_2b_3 - b_2a_3) + \xi(a_2b_4 - b_2a_4) + \eta(a_4b_3 - b_4a_3)$.

References

[1] SPE comparative solution project. Available from: <http://www.spe.org/csp/datasets/set02.htm>.
[2] I. Aavatsmark, An introduction to multi-point flux approximations for quadrilateral grids, Computat. Geosci. 6 (2002) 405–432.
[3] I. Aavatsmark, T. Barkve, Ø. Bøe, T. Mannseth, Discretization on non-orthogonal, curvilinear grids for multi-phase flow, in: Proceedings of the Fourth European Conference on the Mathematics of Oil Recovery, Røros, Norway, 1994.
[4] I. Aavatsmarka, G.T. Eigestad, J.M. Nordbotten, A compact MPFA method with improved robustness, in: Proceedings of the ECMOR X, 5–8 September, Amsterdam, Holland, 2006.
[5] R.E. Bank, D.J. Rose, Some error estimates for the box method, SIAM J. Numer. Anal. 24 (1987) 777–787.
[6] M. Berndt, K. Lipnikov, J. Moulton, M. Shashkov, Convergence of mimetic finite difference discretizations of the diffusion equation, East–West J. Numer. Math. 9 (2001) 253–316.
[7] M. Berndt, K. Lipnikov, M. Shashkov, M. Wheeler, I. Yotov, Superconvergence of the velocity in mimetic finite difference methods on quadrilaterals, SIAM J. Numer. Anal. 43 (4) (2005) 1728–1749.
[8] F. Brezzi, K. Lipnikov, M. Shashkov, Convergence of mimetic finite difference method for diffusion problems on polyhedral meshes, SIAM J. Numer. Anal. 43 (5) (2005) 1872–1896.
[9] F. Brezzi, K. Lipnikov, V. Simoncini, A family of mimetic finite difference methods on polygonal and polyhedral meshes, Math. Mod. Meth. Appl. Sci. 15 (2005) 1533–1553.
[10] Z. Cai, J. Jones, S.F. McCormick, T. Russell, Control volume mixed finite element methods, Computat. Geosci. 1 (1997) 289–315.
[11] Z. Cai, J. Mandel, S.F. McCormick, The finite volume element method for diffusion equations on general triangulations, SIAM J. Numer. Anal. 28 (1991) 392–402.
[12] S.-H. Chou, D.Y. Kwak, K.Y. Kim, A general framework for constructing and analyzing mixed finite volume methods on quadrilateral grids: the overlapping covolume case, SIAM J. Numer. Anal. 39 (4) (2001) 1170–1196.
[13] P.G. Ciarlet, The Finite Element Method for Elliptic Problems, SIAM, Philadephia, PA, 2002.
[14] L.J. Durlofsky, Accuracy of mixed and control volume finite element approximations to darcy velocity and related quantities, Water Resour. Res. 30 (4) (1994) 965–973.
[15] M. Edwards, C. Rogers, A flux-continuous scheme for the full tensor pressure equation, in: Proceedings of the Fourth European Conference on the Mathematics of Oil Recovery, Røros, Norway, 1994.
[16] G. Eigestad, R. Klausen, Convergence of the MPFA O-method: numerical experiments for discontinuous media, Numer. Meth. Part. Differen. Equat. 21 (6) (2005) 1079–1098.
[17] H. Hægland, H. Dahle, F. Eigestad, K.-A. Lie, I. Aavatsmark, Improved streamlines and time-of-flight for streamline simulation of irregular grids, Adv. Water Resour. 30 (4) (2007) 1027–1045.
[18] Z. Heinemann, C. Brand, Gridding techniques in reservoir simulation, in: First and Second International Forum on Reservoir Simul., Alpbach, Austria, 12–16 September, 1998 and 4–8 September, 1989, pp. 339–426.
[19] R. Klausen, T. Russell, Relations among some locally conservative discretization methods which handle discontinuous coefficients, Computat. Geosci. 8 (4) (2004) 341–377.
[20] R.A. Klausen, R. Winther, Convergence of multi-point flux approximations on quadrilateral grids, Numer. Meth. Part. Differen. Equat. 22 (6) (2006) 1438–1454.
[21] Y. Kuznetsov, S. Repin, New mixed finite element method on polygonal and polyhedral meshes, Russ. J. Numer. Anal. Math. Model. 18 (3) (2003) 261–278.
[22] S.H. Lee, H.A. Tchelepi, P. Jenny, L.J. Dechant, Implementation of a flux-continuous finite-difference method for stratigraphic hexahedron grids, SPE J. 7 (3) (2002) 267–277, September 2002, SPE Paper 80117.
[23] S.F. Matringe, R. Juanes, H.A. Tchelepi, Robust streamline tracing for the simulation of porous media flow on general triangular and quadrilateral grids, J. Comput. Phys. 219 (2) (2006) 992–1012.
[24] M. Mlacnik, L. Durlofsky, R. Juanes, H. Tchelepi, Multi-point flux approximations for reservoir simulation. Presented at Twelveth Annual SUPRI-HW Affiliates Meeting, November 18–19, Stanford University, 2004.

[25] R.L. Naff, T.F. Russell, J.D. Wilson, Shape functions for velocity interpolation in general hexahedral cells, Computat. Geosci. 6 (3–4) (2002) 285–314.
[26] A. Njifenjou, I. Nguena, A finite volume approximation for second order elliptic problems with a full matrix on quadrilateral grids: derivation of the scheme and a theoretical analysis, Int. J. Finite Vol. 3 (2) (2006).
[27] J.M. Nordbotten, I. Aavatsmark, Monotonicity conditions for control volume methods on uniform parallelogram grids in homogeneous media, Computat. Geosci. 9 (1) (2005) 61–72.
[28] J.M. Nordbotten, I. Aavatsmarka, G.T. Eigestad, Monotonicity of control volume methods, Numer. Math. 106 (2) (2007) 255–288 (April).
[29] J.M. Nordbotten, G.T. Eigestad, Discretization on quadrilateral grids with improved monotonicity properties, J. Comput. Phys. 203 (2005) 744–760.
[30] B. Rivière, M.F. Wheeler, K. Banaś, Part II, discontinuous Galerkin method applied to a single phase flow in poros media, Computat. Geosci. 4 (4) (2000) 337–349 (December).
[31] H. Royden, Real Analysis, MacMillan, New York, NY, 1988.
[32] T. Schmidt, Box schemes on quadrilateral meshes, Computing 51 (1993) 271–292.
[33] M. Shashkov, S. Steinberg, Solving diffusion equations with rough coefficients in rough grids, J. Comput. Phys. 129 (1996) 383–405.
[34] S. Verma, K. Aziz, A control volume scheme for flexible grids in reservoir simulation, in: SPE Reservoir Simul. Symposium, 8–11 June, Dallas, Texas, 1997, SPE 37999.
[35] X. Wu, R. Parashkevov, Effect of grid deviation on flow solutions, in: SPE Reservoir Simul. Symposium, 31 January–2 February, Houston, Texas, 2005, SPE 92868.